JACS
JOURNAL OF THE AMERICAN CHEMICAL SOCIETY
Communication
pubs.acs.org/JACS

Paramagnetic Nanoparticles Leave Their Mark on Nuclear Spins of Transiently Adsorbed Proteins

Serena Zanzoni,[†] Marco Pedroni,[‡] Mariapina D'Onofrio,[†] Adolfo Speghini,*[,‡] and Michael Assfalg*[,†]

[†]Biomolecular NMR Laboratory, Department of Biotechnology, University of Verona, 37134 Verona, Italy
[‡]Nanomaterials Research Group, Department of Biotechnology, University of Verona and INSTM, 37134 Verona, Italy

Supporting Information

ABSTRACT: The successful application of nanomaterials in biosciences necessitates an in-depth understanding of how they interface with biomolecules. Transient associations of proteins with nanoparticles (NPs) are accessible by solution NMR spectroscopy, albeit with some limitations. The incorporation of paramagnetic centers into NPs offers new opportunities to explore bio−nano interfaces. We propose NMR paramagnetic relaxation enhancement as a new tool to detect NP-binding surfaces on proteins with increased sensitivity, also extending the applicability of NMR investigations to heterogeneous biomolecular mixtures. The adsorption of ubiquitin on gadolinium-doped fluoride-based NPs produced residue-specific NMR line-broadening effects mapping to a contiguous area on the surface of the protein. Importantly, an identical paramagnetic fingerprint was observed in the presence of a competing protein−protein association equilibrium, exemplifying possible interactions taking place in crowded biological media. The interaction was further characterized using isothermal titration calorimetry and upconversion emission measurements. The data indicate that the used fluoride-based NPs are not biologically inert but rather are capable of biomolecular recognition.

Understanding and controlling the interactions of nanoparticles (NPs) with biomolecules is essential for the successful development of novel applications in bionanoscience.[1−3] The description of preferential protein regions that interact with NP surfaces is of high interest, as it contributes to explain the modes of adsorption and the orientation of functional epitopes.[4] Nonetheless, our current understanding of biomolecule−NP interfaces remains limited, and new and refined methodologies are strongly needed.

High expectations have been placed on the use of solution NMR spectroscopy for the characterization of proteins binding to NPs.[5] Important findings relate to NP-induced changes in local stability, structure, and dynamics as well as to the determination of surface coverage and the identification of NP-binding protein surfaces.[6] The description of binding sites can be obtained by monitoring NP-induced protein signal perturbations at the single-residue level in heteronuclear correlation NMR spectra. Under certain kinetic exchange regimes, the observed signals are exchange-mediated and can be used to map the contact surfaces.[5] Chemical shift perturbation (CSP) analyses have been utilized by several research groups for the description of interaction surfaces in a variety of protein−NP pairs.[5,7] As already noted, the method requires caution to avoid interference from protein self-interactions between adsorbing molecules.[7a]

We aimed at exploiting paramagnetic NMR as an additional, or alternative, method to conventional approaches for the investigation of proteins contacting NPs. Paramagnetic effects may provide increased sensitivity due to the strong electron−nucleus interaction. Furthermore, by the use of paramagnetic NPs, protein signal perturbations are expected to report unambiguously on the protein−NP interaction surface regardless of attendant protein−protein associations. Herein we describe the interaction of the model protein ubiquitin (Ub) with rare-earth-doped fluoride-based NPs. Ub has been selected as the test protein in several studies because of its thoroughly characterized behavior in solution. Ub was reported to interact specifically with gold NPs[7b] and to bind citrate-coated silver NPs.[7c] The adsorption of Ub onto pristine silver NPs resulted in the formation of amyloid-like structures.[7c] Ub was further shown to form reversible soluble aggregates with fullerenol clusters, thereby inhibiting the enzyme-catalyzed synthesis of polyUb chains.[7d]

Lanthanide (Ln)-doped fluoride NPs have been intensely investigated in recent years as attractive materials for biomedical applications,[8] in particular in relation to their unique luminescence properties, such as upconversion (UC) emission.[9] UC is extremely useful for in vivo imaging, enabling deep tissue penetration, minimal tissue scattering, and high optical imaging resolution.[10] Despite their extraordinary potential for applications in nanomedicine, the characterization of the interactions between Ln-doped fluoride NPs and biomolecules remains scarce. In this work, we focused on SrF_2 NPs because of their excellent features as luminescent materials, as demonstrated by very efficient UC of Tm/Yb and Er/Yb codoped samples.[11]

The composition and size of SrF_2 NPs can be tuned at will to best suit diverse experiments. In the present investigation, citrate-stabilized, water-dispersible core and core@shell NPs with sizes of 10−12 nm were prepared (see Experimental Details and Figure S1 in the Supporting Information). Ub adsorption to NPs was first explored using 1D solution ^{1}H NMR experiments, a valuable tool for detecting interaction processes.[6b] For these experiments, we used SrF_2:Y^{3+} NPs (Sr:Y

Received: November 5, 2015
Published: December 18, 2015

ACS Publications © 2015 American Chemical Society

DOI: 10.1021/jacs.5b11582
J. Am. Chem. Soc. 2016, 138, 72−75

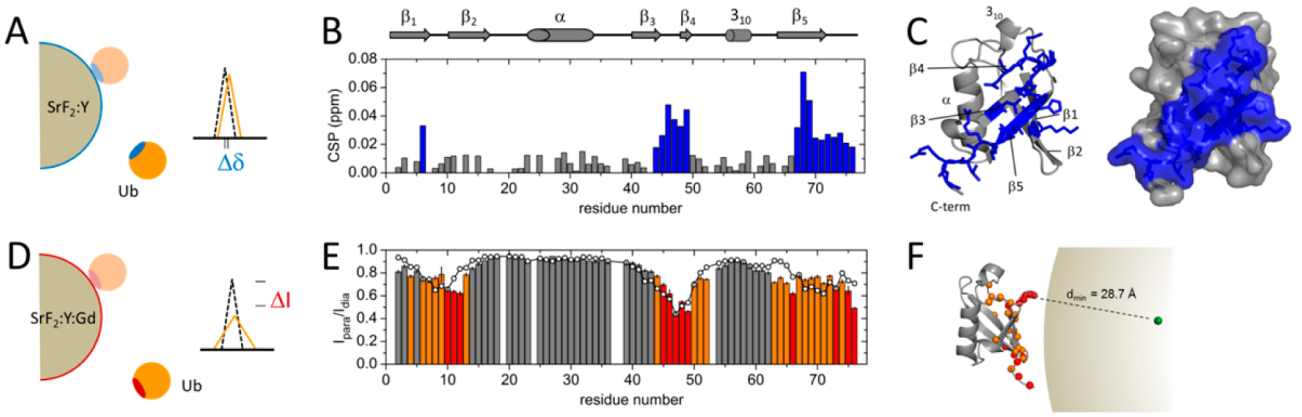

Figure 1. NMR perturbation mapping in Ub/NP mixtures. (A–C) CSP mapping. (A) Schematic picture illustrating the site-specific peak position changes observed for Ub upon transient adsorption to diamagnetic NPs. (B) Residue-specific CSPs observed on 100 μM Ub after addition of 7.2 μM SrF_2:Y NPs. CSPs > 0.02 ppm are highlighted in blue. The secondary structure elements are shown at the top. (C) Cartoon (left) and molecular surface (right) representations of Ub, reporting in blue the residues experiencing large CSPs. Secondary structure elements are indicated. (D–F) PRE mapping. (D) Schematic picture illustrating the site-specific peak intensity changes observed for Ub upon transient adsorption to paramagnetic NPs. (E) Backbone amide ^{1}H,^{15}N-HSQC peak intensity perturbations measured on 100 μM Ub in the presence of 0.6 μM paramagnetic SrF_2:Y,Gd NPs (I_{para}) compared with those measured using diamagnetic SrF_2:Y NPs (I_{dia}). Residue-specific I_{para}/I_{dia} ratios are plotted as bars vs the primary sequence. Errors were estimated from spectral noise. Strong perturbations are highlighted in red and medium perturbations in orange, and the remaining data are shown in gray. Open circles correspond to predicted I_{para}/I_{dia} values. (F) Pictorial view of Ub binding to SrF_2 NPs. Ub is displayed in cartoon representation, and atoms of residues experiencing strong (red) or medium (orange) PREs are shown as spheres. The calculated position of a Gd^{3+} metal center within the NP is indicated by a green sphere. The distance of closest approach, separating H_N of Gly47 from a Gd^{3+} ion, is displayed. The shaded area represents a portion of the NP.

= 0.78:0.22), in which only diamagnetic ions were present (Figure 1A). A progressive overall protein signal attenuation was observed upon addition of NPs (Figure S2A), consistent with the formation of Ub–NP assemblies not directly detectable by NMR spectroscopy.[5] Moreover, we acquired 2D correlation spectra (^{1}H,^{15}N-HSQC), in which every protein amide group is revealed as a 2D peak and its CSP used as reporter of the interaction. Small CSPs were observed in late titration steps (Figure S2C). With the aid of line shape simulation software, we estimated a dissociation rate constant on the order of 100–300 s^{-1} and a dissociation constant (K_d) of 2.4 ± 2.2 μM (Experimental Details and Figure S3). CSPs were found to vary along the protein sequence, with the strongest perturbations localizing to discrete polypeptide stretches 44–49 (strands β_3 and β_4) and 67–75 (β_5) as well as at position 6 (β_1) (Figure 1B). These residues mapped to a contiguous area of 1100 Å^2 on the surface of Ub (Figure 1C). The residues perturbed in the presence of SrF_2 NPs were either neutral/hydrophobic (Ile44, Phe45, Ala46, Gly47, Gln49, Leu67, Leu69, Val70, Leu71, Leu73, Gly75) or positively charged (Lys6, Lys48, His68, Arg72, Arg74), suggesting that electrostatic attraction with negative charges on the NP surface and hydrophobic effects contributed to the free energy of binding. An analogous surface patch was previously shown to mediate the association of Ub to fullerenol clusters.[7d] Thus, SrF_2 NPs may act similarly to fullerenol by binding to recognition sites that are functional for intracellular communication mediated by Ub.

In addition to the use of conventional NMR methods, paramagnetic Ln-doped NPs offer unique opportunities for the study of reversible protein adsorption. Indeed, paramagnetic ions may cause pronounced effects on the NMR spectra of interacting biomolecules, including contributions to nuclear spin relaxation rates and chemical shifts (Figure 1D). In our work, we chose to exploit SrF_2:Y^{3+},Gd^{3+} NPs (Sr:Y:Gd = 0.78:0.21:0.01). The half-filled 4f orbitals of Gd^{3+} ($S = {}^7/_2$) provide the largest isotropic magnetic susceptibility among all Ln ions and display slow electron spin relaxation.[12] These features translate into a strong paramagnetic relaxation rate enhancement (PRE) of nearby nuclear spins, which can be measured as differences in NMR spectra recorded in the presence of paramagnetic and diamagnetic NPs (Figure S4).[13] The transverse PRE (Γ_2) originates from dipolar interaction mechanisms, shows a proton–electron distance dependence of r^{-6}, and is orientation-independent.[14]

We recorded two sets of ^{1}H,^{15}N-HSQC spectra of Ub in the presence of either SrF_2:Y^{3+},Gd^{3+} or SrF_2:Y^{3+} NPs at identical NP additions. The ratios of peak heights measured for the paramagnetic and diamagnetic samples, I_{para}/I_{dia}, are related to the residue-specific ^{1}H Γ_2 and therefore to the individual amide proton–metal center distances.[15] By plotting the I_{para}/I_{dia} values against the protein sequence (Figure 1E), we observed pronounced intensity attenuations in defined polypeptide stretches, particularly 4–13 (β_1 and β_2), 44–52 (β_3 and β_4), and 63–76 (β_5). The residues experiencing strong PREs map to a contiguous area on the protein surface (Figure 1F), approximately centered around strand β_5 and located opposite to the α-helix. The observation of perturbations confined to this particular face of the protein structure is a clear indication that Ub interacts specifically with the NPs, confirming the result obtained by CSP analysis. Differences in the regions identified with the two methods may be ascribed to the distinct nature of the perturbation phenomena (i.e., altered local chemical environment for chemical shifts vs distance from unpaired electrons in the case of PREs). We note that PREs are long-range effects, thus possibly extending beyond the atoms in direct contact with the NP surface.

In order to gain further insight into possible orientations of the protein molecules with respect to the NP surface, we analyzed the experimental intensity attenuations, seeking the position of a Gd^{3+} ion that would best satisfy the PRE constraints. The location of the metal center with respect to the

DOI: 10.1021/jacs.5b11582
J. Am. Chem. Soc. 2016, 138, 72–75

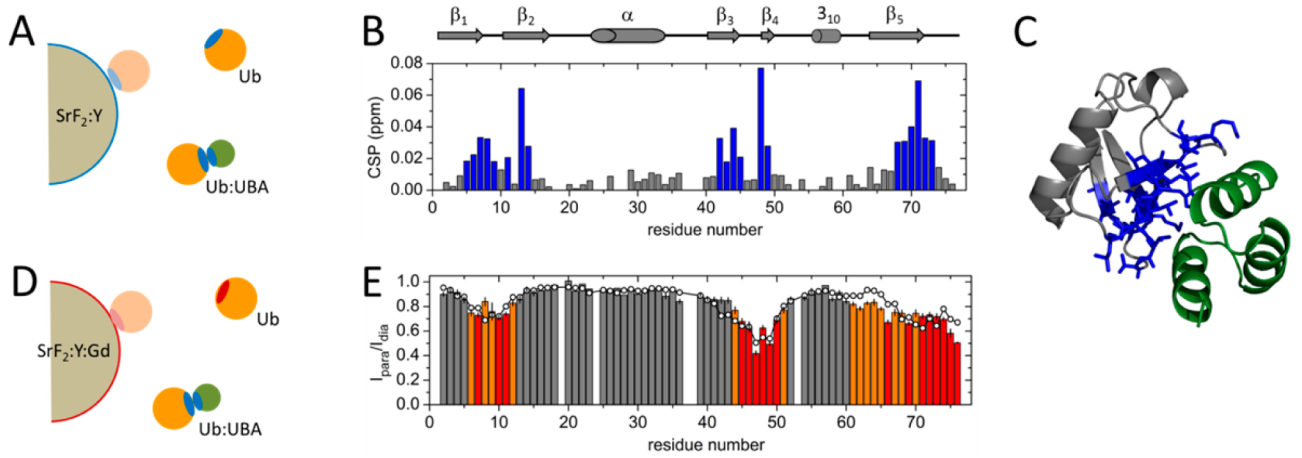

Figure 2. NMR perturbation mapping in Ub/UBA/NP mixtures. (A–C) CSP mapping. (A) Schematic picture illustrating the site-specific peak position changes observed for Ub upon transient interaction with diamagnetic NPs and UBA. (B) Residue-specific CSPs observed on a 100 μM Ub/500 μM UBA mixture after addition of 9.1 μM SrF_2:Y NPs. CSPs > 0.02 ppm are highlighted in blue. Secondary structure elements are shown at the top. (C) Cartoon representation of the Ub (gray)–UBA (green) complex, reporting in blue the residues experiencing large CSPs. (D–F) PRE mapping. (D) Schematic picture illustrating the site-specific peak intensity changes observed for Ub upon transient adsorption to paramagnetic NPs in the presence of UBA. (E) ^{1}H,^{15}N-HSQC peak intensity perturbations (I_{para}) measured on a 100 μM Ub/500 μM UBA mixture in the presence of 11.7 μM SrF_2 NPs (0.8 SrF_2:Y, 0.2 SrF_2:Y,Gd) compared with those measured with diamagnetic SrF_2 NPs (I_{dia}). Residue-specific I_{para}/I_{dia} ratios are plotted as bars vs the primary sequence, together with estimated experimental errors. Strong perturbations are shown in red and medium perturbations in orange, and the remaining data are shown in gray. Open circles correspond to predicted I_{para}/I_{dia} values.

protein was determined by using a 3D search procedure that minimizes the differences between the experimentally measured and predicted values of I_{para}/I_{dia} for each amino acid residue (Figure 1F and Table S1).[16] The calculation was performed using the equations valid under fast exchange (on the relaxation time scale).[17] The trend of the back-calculated I_{para}/I_{dia} values approximately followed the sequence-dependent variability of the experimental data (Figure 1E), correctly reproducing the absence of PRE in the 16–40 and 57–59 stretches and the strong intensity attenuation for the region centered around residue 47. Some inconsistency was found in the 11–12 and 63–66 segments. At least the following situations may justify the observations: (i) each protein molecule may come into close proximity of a single Gd^{3+} ion close to the NP surface but (a) the center of the same contacting interface in distinct molecules may be separated by different distances from the paramagnetic center or (b) the binding epitope may not be exactly the same for each Ub molecule; (ii) each Ub molecule may experience the combined effect of more than one Gd^{3+} ion, which may be (a) homogeneously or (b) inhomogeneously distributed within the external NP shell; (iii) the structure of NP-bound Ub may not correspond exactly to that of the X-ray structure used in the calculations; (iv) a combination of the above. Presumably, NP-bound Ub is best represented by an ensemble of similar orientational states, one of the most significant being displayed in Figure 1F as obtained from our calculation.

The convincing PRE mapping obtained using Ub stimulated us to evaluate the power of the method in identifying NP-binding sites of proteins in the presence of attendant protein–protein interactions. Because Ub has a very low tendency to self-aggregate, the occurrence of homotypic complexes either in solution or at the NP surface is difficult to grasp. For a better demonstration, we chose to focus on heterotypic associations (Figure 2A), which represent probable events in crowded biological media. Ub is known to interact weakly (K_d ~ 400 μM) with the Ub-associated 2 (UBA) domain of hHR23A.[18] The UBA contacting surface has been previously identified as the Leu8-Ile44-Val70 Ub patch,[18] which is large part overlaps with the Ub–NP interaction surface. On the basis of 1D ^{1}H NMR experiments, UBA was found not to interact significantly with SrF_2 NPs (Figure S2B). Upon addition of SrF_2:Y^{3+} NPs to a preformed 1:5 Ub:UBA mixture (corresponding to ~60% saturation of Ub), specific CSPs were observed (Figure 2B,C), and the subsequent addition of SrF_2:Y^{3+},Gd^{3+} NPs yielded localized signal intensity attenuations (Figure 2D,E). The observed CSPs can be attributed to both direct Ub–NP interactions as well as a redistribution of Ub and Ub/UBA fractional populations as a consequence of the transition from a two-state to a three-state dynamic equilibrium, characterized by a single set of exchange-averaged peak positions. Thus, the CSP pattern collects contributions from the interactions of Ub with both the NP and the protein partner (Figures 2B and S5). Conversely, the PRE pattern, showing large agreement with that observed for Ub alone, maps the NP-binding region only. As a confirmation, the corresponding back-calculated intensities (Figure 2E) are virtually identical to those predicted for Ub alone (Figure 1E).

Given the strong interest in the UC phenomenon, we also investigated UC emission in the presence of Ub. We adopted the Tm/Yb codoping strategy for strong UC emission, which can be efficiently activated by NIR excitation (at around 980 nm) into the $^2F_{5/2}$ energy level of the Yb^{3+} ions. For best sensitivity, the NP core was activated with Yb^{3+} while the shell was codoped with Yb^{3+} and Tm^{3+}. The SrF_2:Yb@SrF_2:Yb,Tm core@shell architecture ensures efficient absorption of the NIR radiation by Yb^{3+} in both the core and shell and guarantees that a significant amount of Tm^{3+} ions are located at the NPs surface. We followed the UC in the visible and NIR regions (450–850 nm range) upon addition of Ub in D_2O (Figure S6). A clear decrease in the UC of the NPs was observed, attributable to altered efficiency of nonradiative processes due to multiphonon relaxation.[11a] Since the phonon energies for N–D groups are very similar to those for O–D groups,[19]

DOI: 10.1021/jacs.5b11582
J. Am. Chem. Soc. 2016, 138, 72–75

vibrations involving C−H groups are most likely responsible for decreasing the radiative emission. We observed a decrease in UC intensity by a significant 9−11% at saturation (Table S2).

The thermodynamics of the Ub−NP interaction was investigated using isothermal titration calorimetry (Experimental Details and Figure S7). The binding equilibrium was characterized by an unfavorable enthalpic contribution (ΔH = 224 ± 13 kJ mol^{-1}), offset by a favorable entropic contribution (ΔS = 853 J K^{-1} mol^{-1}) to the total free energy change (ΔG = −30 kJ mol^{-1}, derived from the determined K_d value of 6.0 ± 0.6 μM). The positive ΔH may originate from loss of solvent intermolecular interactions around the solutes and/or disruption of water−protein and water−NP contacts that outclass favorable Ub−NP polar interactions. The positive ΔS can be attributed to increased disorder of the solvent molecules. Moreover, rearrangement of the dispersant could contribute with an additional energy term.

In conclusion, we have described an investigation of biomolecular interactions with Ln-doped NPs representing an example of UCNPs with promising potential applications in biomedicine. Using site-resolved CSP and PRE mapping, we have identified a very specific contact surface on Ub, suggesting that the used NPs are potentially bioactive and could associate with biomolecules such as plasma proteins. Moreover, we have extended the scope of the NMR technique in protein−NP interaction studies exploiting the unique properties of paramagnetic Ln ions. Paramagnetic ions close to the surface of NPs imprint metal−nucleus distance information on NMR spectra of adsorbing proteins. PRE mapping improves the sensitivity of binding-site detection by NMR spectroscopy and has the unique advantage over alternative strategies that NP-contacting sites can also be detected when the test protein experiences competing interactions with itself (aggregation) or with other components of complex macromolecular mixtures (e.g., biological media). However, both CSP and PRE mapping are applicable only to weak protein−NP interactions. Gd is particularly suited for PRE measurements, and GdF_3 NPs have been proposed as useful relaxation agents in NMR/MRI studies.[20] In principle, paramagnetic effects can be tuned at will, exploiting the versatility of Ln ions, which are characterized by similar chemistry but different magnetic properties.[13] The proposed approach is of general applicability to all NP systems that intrinsically incorporate paramagnetic metals or in which paramagnetic ions, metal chelates, or organic spin labels can be introduced.

■ ASSOCIATED CONTENT

Supporting Information

The Supporting Information is available free of charge on the ACS Publications website at DOI: 10.1021/jacs.5b11582.

Experimental procedures, Tables S1 and S2, and Figures S1−S7 (PDF)

■ AUTHOR INFORMATION

Corresponding Authors

*adolfo.speghini@univr.it
*michael.assfalg@univr.it

Notes

The authors declare no competing financial interest.

■ ACKNOWLEDGMENTS

We thank "Centro Grandi Attrezzature di Ateneo" for NMR spectrometer maintenance.

■ REFERENCES

(1) Mahmoudi, M.; Lynch, I.; Ejtehadi, M. R.; Monopoli, M. P.; Bombelli, F. B.; Laurent, S. *Chem. Rev.* **2011**, *111*, 5610.

(2) Gagner, J. E.; Shrivastava, S.; Qian, X.; Dordick, J. S.; Siegel, R. W. *J. Phys. Chem. Lett.* **2012**, *3*, 3149.

(3) Moyano, D. F.; Rotello, V. M. *Nanomedicine* **2014**, *9*, 1905.

(4) Monopoli, M. P.; Aberg, C.; Salvati, A.; Dawson, K. A. *Nat. Nanotechnol.* **2012**, *7*, 779.

(5) Assfalg, M.; Ragona, L.; Pagano, K.; D'Onofrio, M.; Zanzoni, S.; Tomaselli, S.; Molinari, H. *Biochim. Biophys. Acta, Proteins Proteomics* **2016**, *1864*, 102.

(6) (a) Lundqvist, M.; Sethson, I.; Jonsson, B.-H. *Biochemistry* **2005**, *44*, 10093. (b) Wang, A.; Vangala, K.; Vo, T.; Zhang, D.; Fitzkee, N. C. *J. Phys. Chem. C* **2014**, *118*, 8134. (c) Ceccon, A.; Lelli, M.; D'Onofrio, M.; Molinari, H.; Assfalg, M. *J. Am. Chem. Soc.* **2014**, *136*, 13158. (d) Brancolini, G.; Corazza, A.; Vuano, M.; Fogolari, F.; Mimmi, M. C.; Bellotti, V.; Stoppini, M.; Corni, S.; Esposito, G. *ACS Nano* **2015**, *9*, 2600.

(7) (a) Shrivastava, S.; McCallum, S. A.; Nuffer, J. H.; Qian, X.; Siegel, R. W.; Dordick, J. S. *Langmuir* **2013**, *29*, 10841. (b) Calzolai, L.; Franchini, F.; Gilliland, D.; Rossi, F. *Nano Lett.* **2010**, *10*, 3101. (c) Mangini, V.; Dell'Aglio, M.; Stradis, A. D.; Giacomo, A. D.; Pascale, O. D.; Natile, G.; Arnesano, F. *Chem. - Eur. J.* **2014**, *20*, 10745. (d) Zanzoni, S.; Ceccon, A.; Assfalg, M.; Singh, R. K.; Fushman, D.; D'Onofrio, M. *Nanoscale* **2015**, *7*, 7197. (e) Lundqvist, M.; Sethson, I.; Jonsson, B.-H. *Langmuir* **2005**, *21*, 5974.

(8) (a) Prodi, L.; Rampazzo, E.; Rastrelli, F.; Speghini, A.; Zaccheroni, N. *Chem. Soc. Rev.* **2015**, *44*, 4922. (b) Vuojola, J.; Soukka, T. *Methods Appl. Fluoresc.* **2014**, *2*, 012001.

(9) (a) Sedlmeier, A.; Gorris, H. H. *Chem. Soc. Rev.* **2015**, *44*, 1526. (b) Chan, E. M.; Han, G.; Goldberg, J. D.; Gargas, D. J.; Ostrowski, A. D.; Schuck, P. J.; Cohen, B. E.; Milliron, D. J. *Nano Lett.* **2012**, *12*, 3839. (c) Suffren, Y.; Zare, D.; Eliseeva, S. V.; Guénée, L.; Nozary, H.; Lathion, T.; Aboshyan-Sorgho, L.; Petoud, S.; Hauser, A.; Piguet, C. *J. Phys. Chem. C* **2013**, *117*, 26957.

(10) Smith, A. M.; Mancini, M. C.; Nie, S. *Nat. Nanotechnol.* **2009**, *4*, 710.

(11) (a) Pedroni, M.; Piccinelli, F.; Passuello, T.; Polizzi, S.; Ueda, J.; Haro-González, P.; Martinez Maestro, L.; Jaque, D.; García-Solé, J.; Bettinelli, M.; Speghini, A. *Cryst. Growth Des.* **2013**, *13*, 4906. (b) Quintanilla, M.; Cantarelli, I. X.; Pedroni, M.; Speghini, A.; Vetrone, F. *J. Mater. Chem. C* **2015**, *3*, 3108.

(12) Bertini, I.; Luchinat, C. *Coordination Chemistry Reviews, Vol. 150*; Elsevier: Amsterdam, 1996.

(13) Otting, G. *Annu. Rev. Biophys.* **2010**, *39*, 387.

(14) Clore, G. M.; Iwahara, J. *Chem. Rev.* **2009**, *109*, 4108.

(15) Battiste, J. L.; Wagner, G. *Biochemistry* **2000**, *39*, 5355.

(16) D'Onofrio, M.; Gianolio, E.; Ceccon, A.; Arena, F.; Zanzoni, S.; Fushman, D.; Aime, S.; Molinari, H.; Assfalg, M. *Chem. - Eur. J.* **2012**, *18*, 9919.

(17) Anthis, N. J.; Clore, G. M. *Q. Rev. Biophys.* **2015**, *48*, 35.

(18) Varadan, R.; Assfalg, M.; Fushman, D. *Methods Enzymol.* **2005**, *399*, 177.

(19) Snels, M.; Fusina, L.; Hollenstein, H.; Quack, M. *Mol. Phys.* **2000**, *98*, 837.

(20) (a) Evanics, F.; Diamente, P. R.; van Veggel, F. C. J. M.; Stanisz, G. J.; Prosser, R. S. *Chem. Mater.* **2006**, *18*, 2499. (b) Passuello, T.; Pedroni, M.; Piccinelli, F.; Polizzi, S.; Marzola, P.; Tambalo, S.; Conti, G.; Benati, D.; Vetrone, F.; Bettinelli, M.; Speghini, A. *Nanoscale* **2012**, *4*, 7682−9.

DOI: 10.1021/jacs.5b11582
J. Am. Chem. Soc. 2016, 138, 72−75